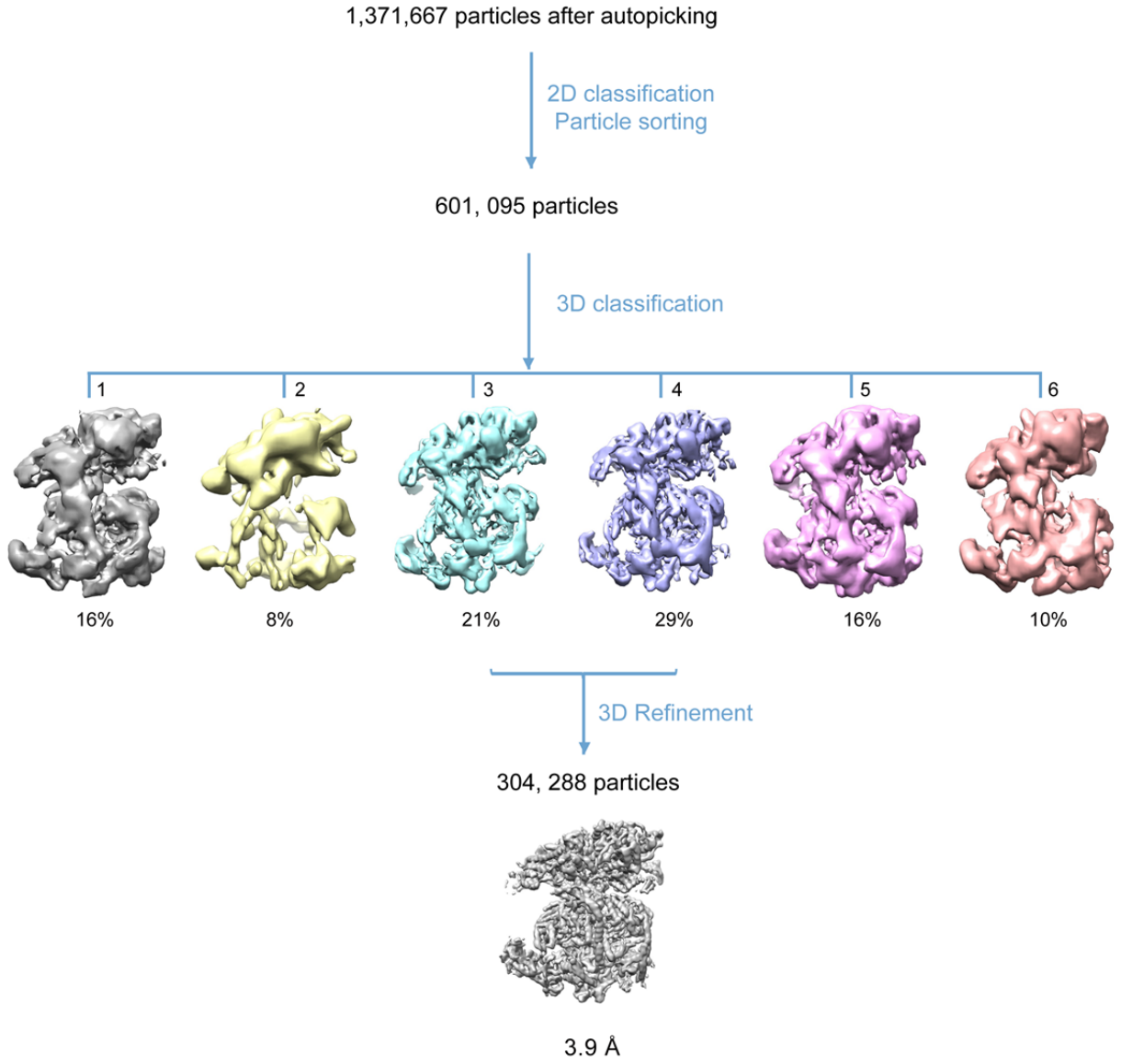
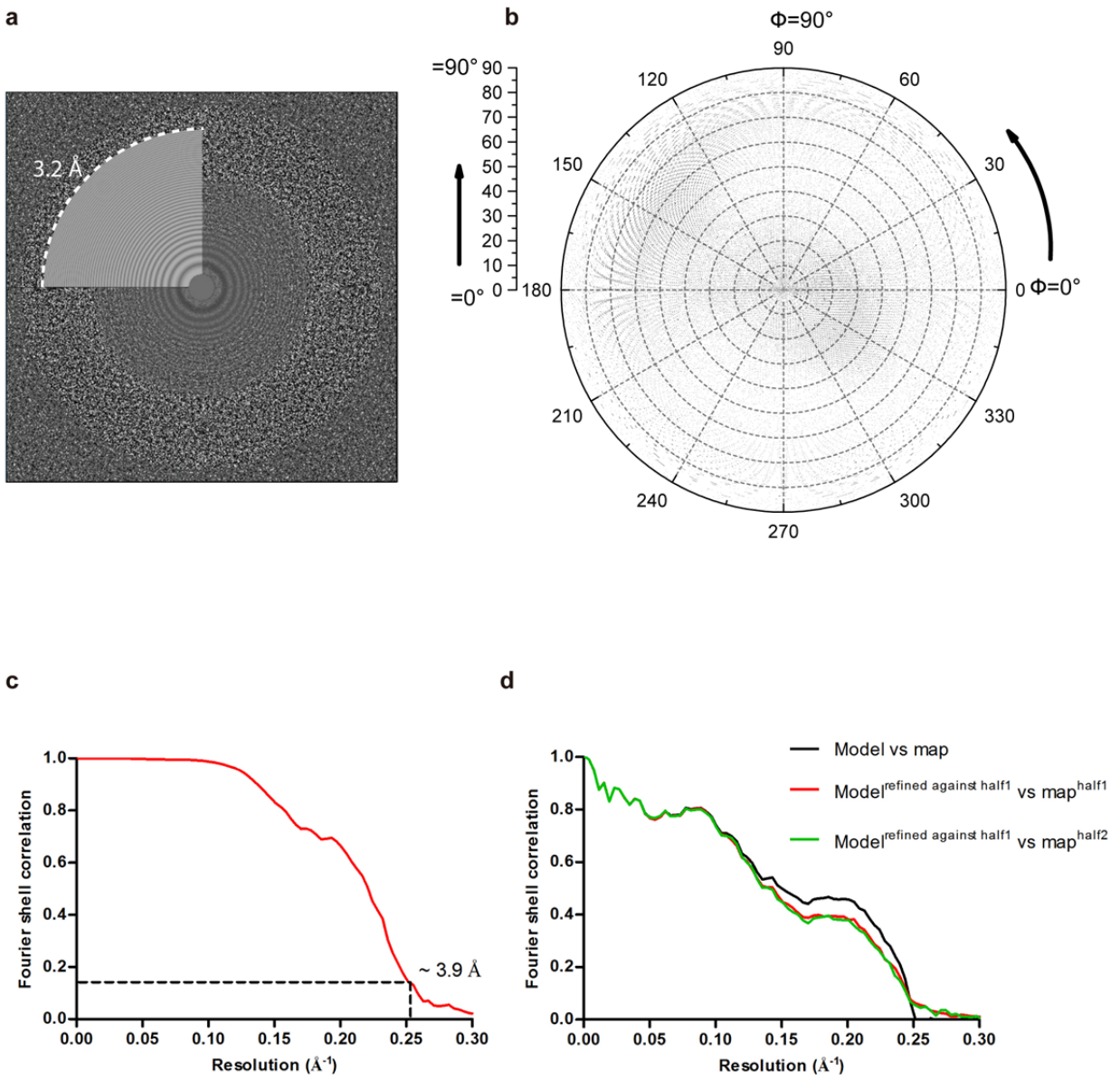
Supplementary Table 1. Cryo-EM data collection and refinement statistics

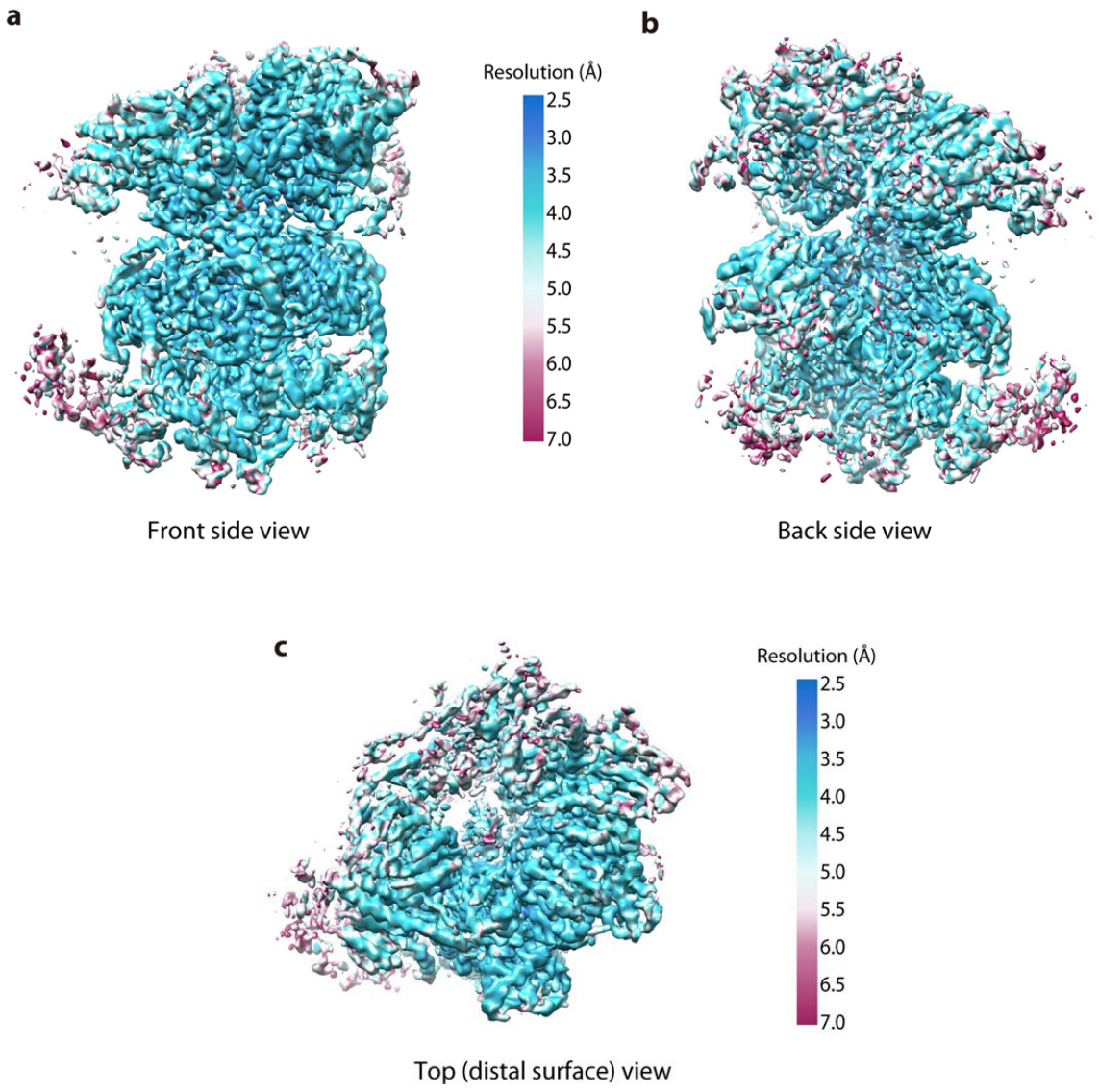
Data Collection	
EM equipment	FEI Titan Krios
Voltage (kV)	300
Detector	Gatan K2
Pixel size (Å)	1.01
Electron dose (e^-/Å^2)	50
Defocus range (μm)	1.5~3.5
Reconstruction	
Software	RELION 1.4
Number of used Particles	304,288
Resolution (Å)	3.9
Map sharpening B-factor (Å^2)	123
Model composition	
Peptide chains	14
Protein residues	6907
Nucleotides	78
R.m.s deviations	
Bonds length (Å)	0.007
Bonds Angle (°)	1.292
Ramachandran plot	
Preferred (%)	89.00
Allowed (%)	9.52
Outlier (%)	1.48
Validation	
Molprobity score	2.56 (98%)
Good rotamer (%)	93.58
Clashscore, all atoms	27.74 (86%)



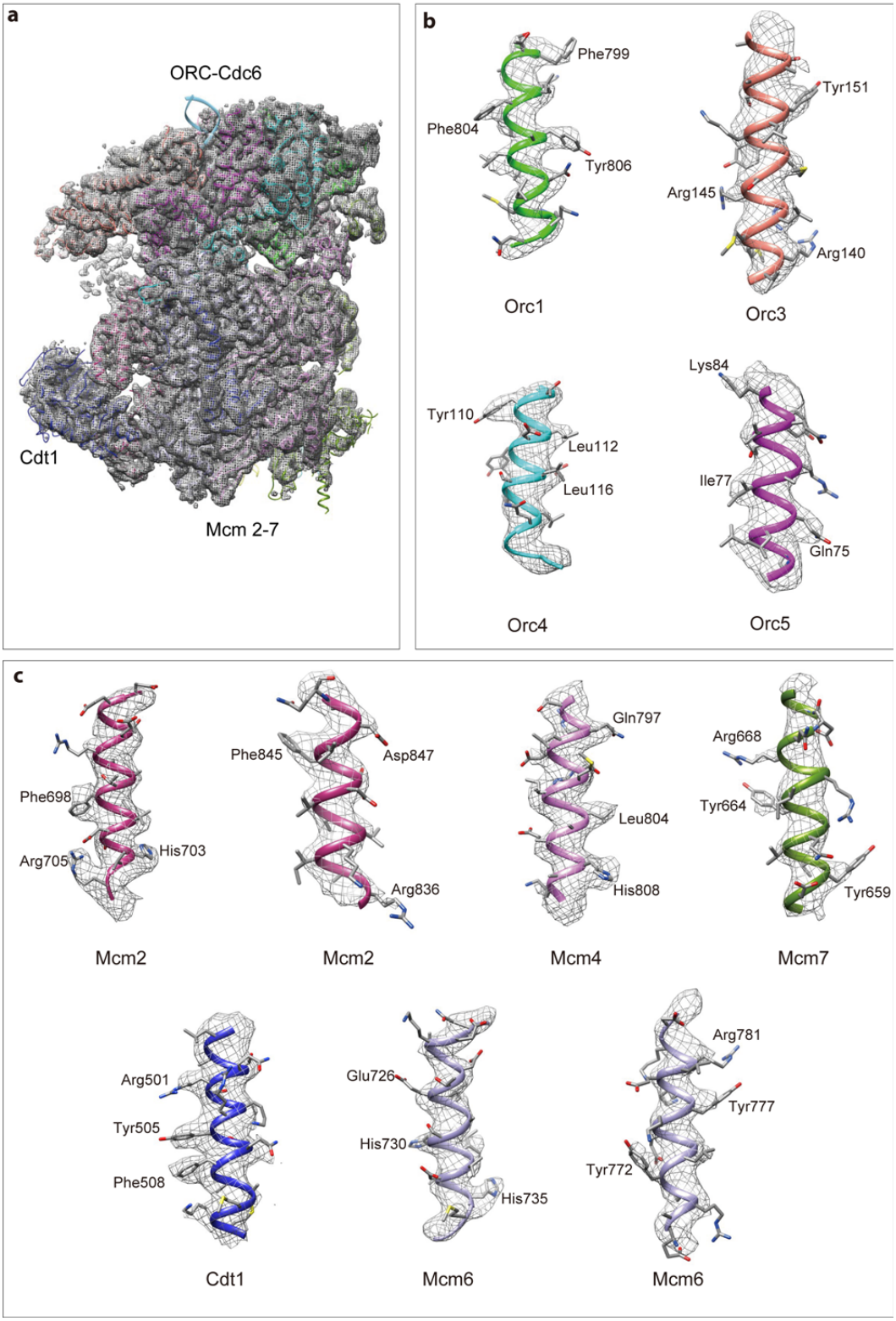
Supplementary Fig. 1. Cryo-EM image processing and 3D reconstruction procedure. Motion-corrected raw particle images were sorted first by 2D classification. After removing raw particles that did not produce "good" averages, about 600,000 particles remained. These particles were further sorted into six 3D classes. Finally, particles that produced the best two 3D classes were combined, yielding ~300,000 particles for final 3D refinement. The final 3D map had an estimated resolution of 3.9 Å.



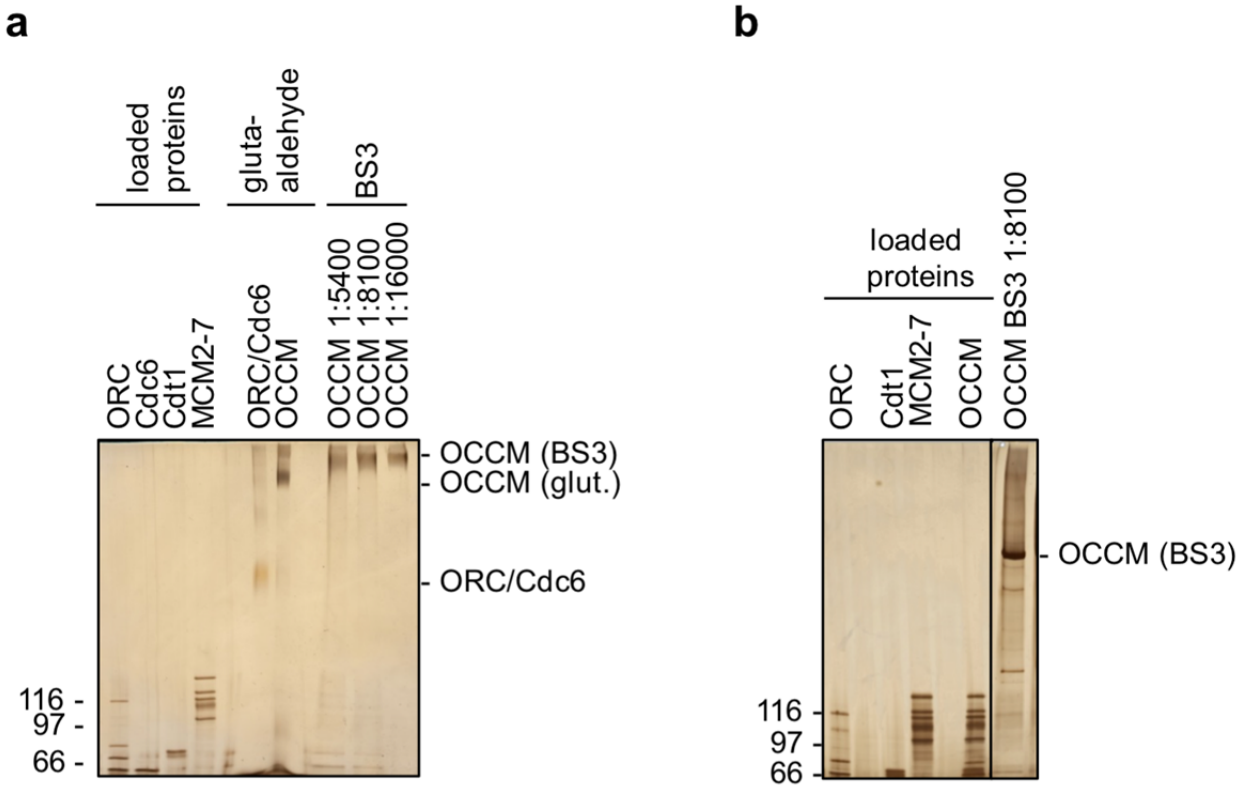
Supplementary Fig. 2. Image resolution, particle Euler angle distribution and FSC. (a) Thon rings in the power spectra of a typical drift-corrected electron micrograph reached to 3.2 Å resolution. The upper left quadrant is a calculated version using the same CTF parameters as found in the experimental image. (**b**) The particle orientation covers all angular space. (**c**) Gold-standard Fourier correlation of two independent half maps. (**d**) Fourier shell correlations of the atomic model with the full 3D map (black), and the correlations of the 0.1-Å randomized and refined model against half map 1 (red), and with half map 2 (green), respectively. The 3.9 Å atomic model was randomly displaced by 0.1 Å. The noise-added model was refined by one round of coordinate and one round of b-factor refinement against half map 1. The refined coordinates were used to calculate FSC with half map 1, half map 2 and the full map respectively. The similarity between these curves indicates the atomic model is not over refined.



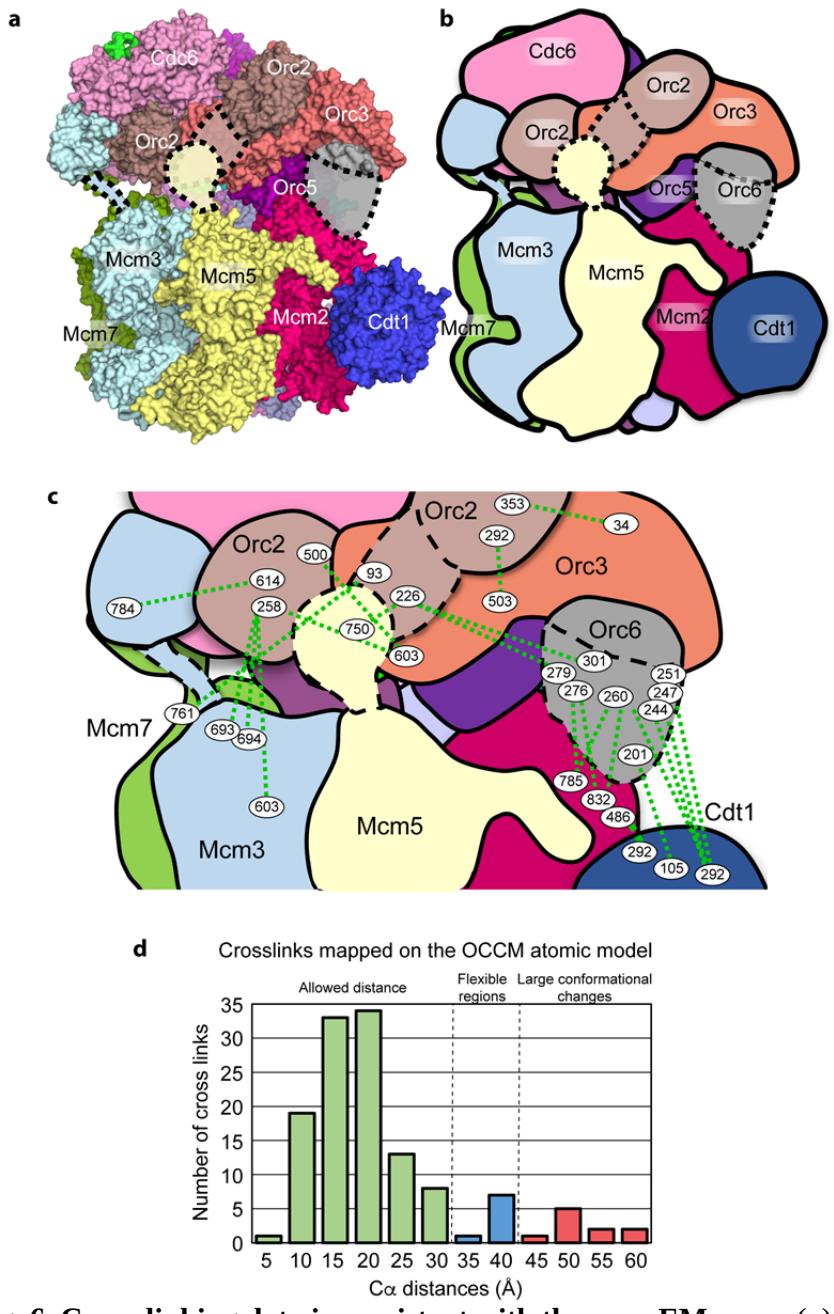
Supplementary Fig. 3. Local resolution map of the cryo-EM structure of the OCCM complex in front side view (a), back side view (b), and top ORC-Cdc6 view (c).



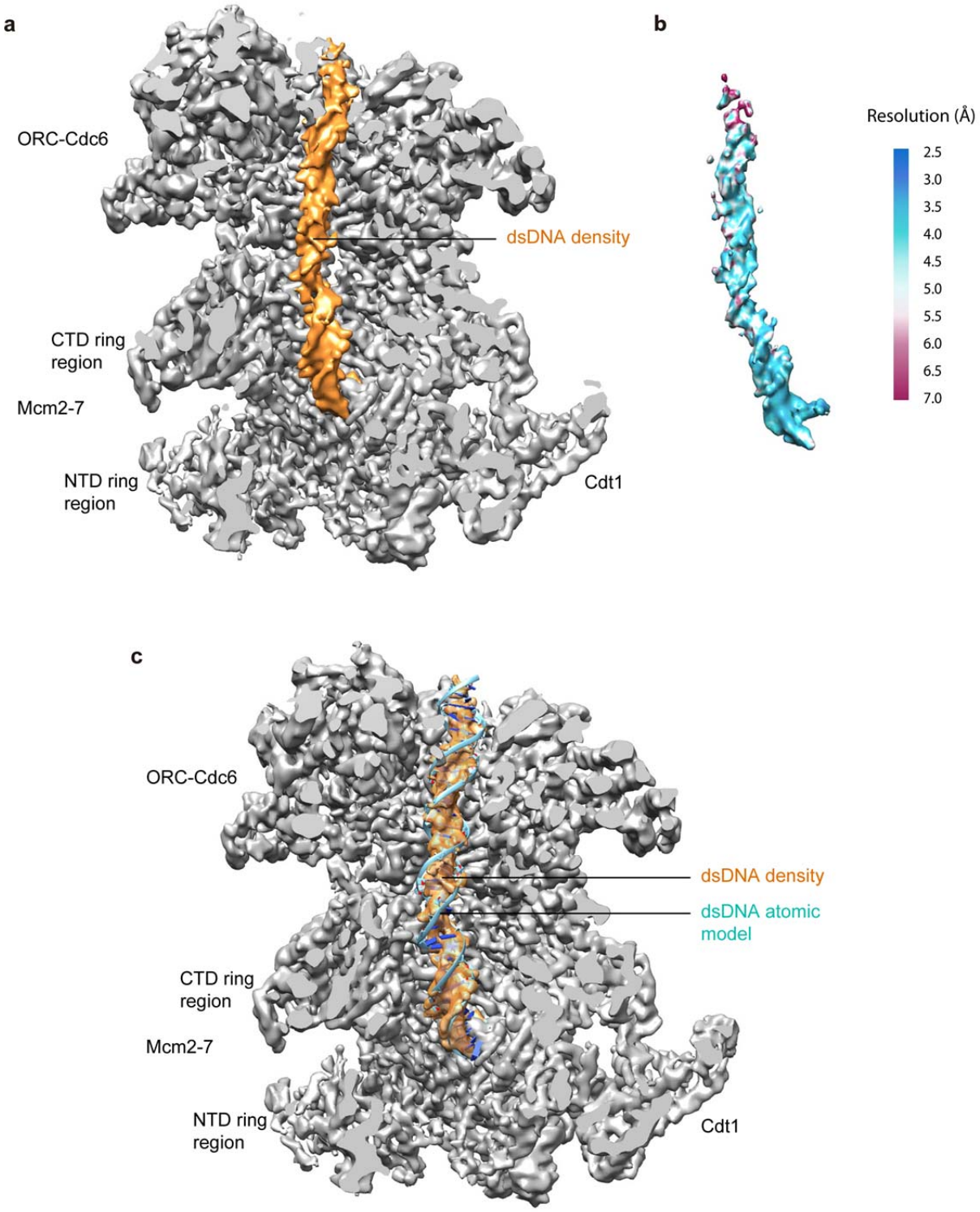
Supplementary Fig. 4. Fitting of the atomic model with the cryo-EM density. (**a**) Overall fitting of the OCCM model with the 3D map. (**b**) Fitting of four selected α-helices in ORC region. (**c**) Fitting of seven selected α-helices in the Cdt1-Mcm2-7 region.



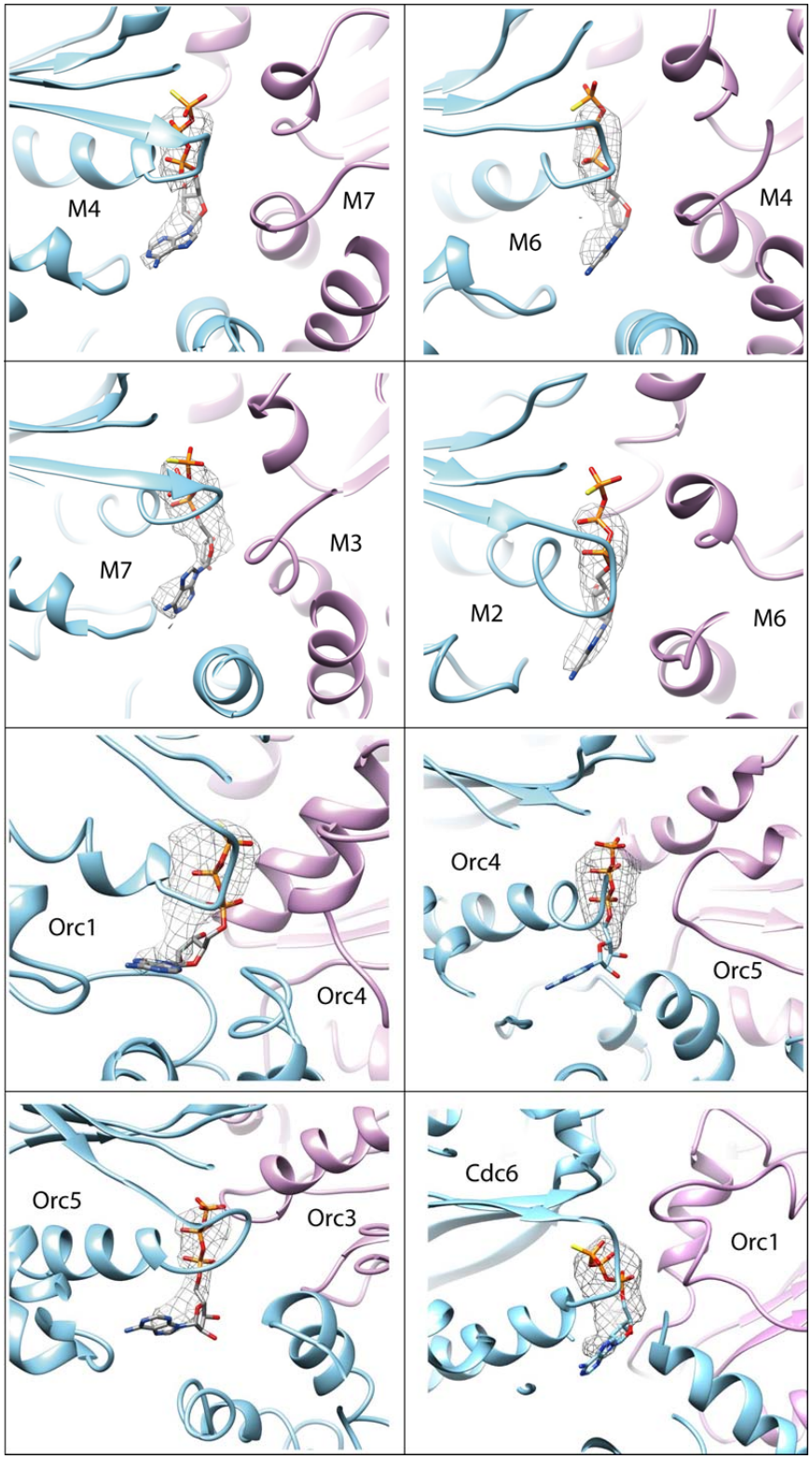
Supplementary Fig. 5. Titration for Cross-linking/Mass Spectrometry. (**a**) After a titration using a wide range of BS3 proportions, it was estimated that the best results were obtained between 1:5400 and 1:16000 protein-crosslinker ratios compared with the OCCM crosslinked with 2% glutaraldehyde. (**b**) Ten microliters of the final crosslinking reaction were run on a SDS PAGE before the Cross-linking/Mass Spectrometry analysis to confirm the homogeneity of the sample.



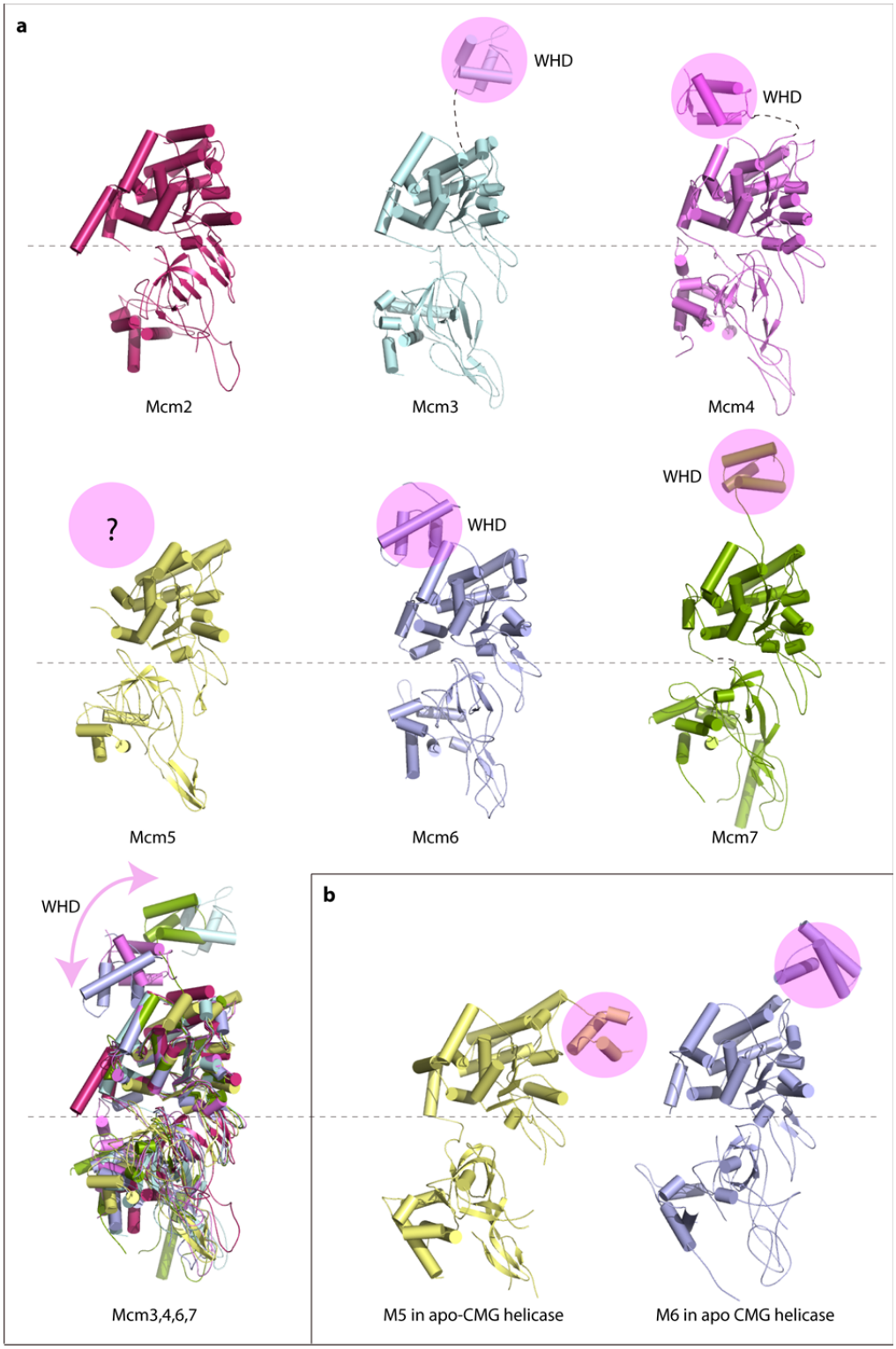
Supplementary Fig. 6. Cross-linking data is consistent with the cryo-EM map. (**a**) Atomic model of *S. cerevisiae* OCCM complex shown in surface view. The regions of Orc6 (grey), Mcm5 (yellow) and Orc2 (brown) that were not resolved in the atomic model, but covered with the cross-linking data are displayed as flat semi-transparent 2D surfaces delimited by a dashed line. The connector between the main body of Mcm3 and the Winged Helix Domain of the protein is presented in the same style. **(b)** A sketch of the OCCM structure in the same view as in (**a**). (**c**) Cross-links between ORC-Cdc6 and Cdt1-Mcm2-7 are shown as dashed green lines. (**d**) Histogram of alpha-carbon distances of observed cross-links as measured in the atomic model of the OCCM. Around 86% of the observed cross-links are within the allowed distance (less than 30 Å) while the rest can be explained due to the presence of flexible regions or large conformational changes in the complex.



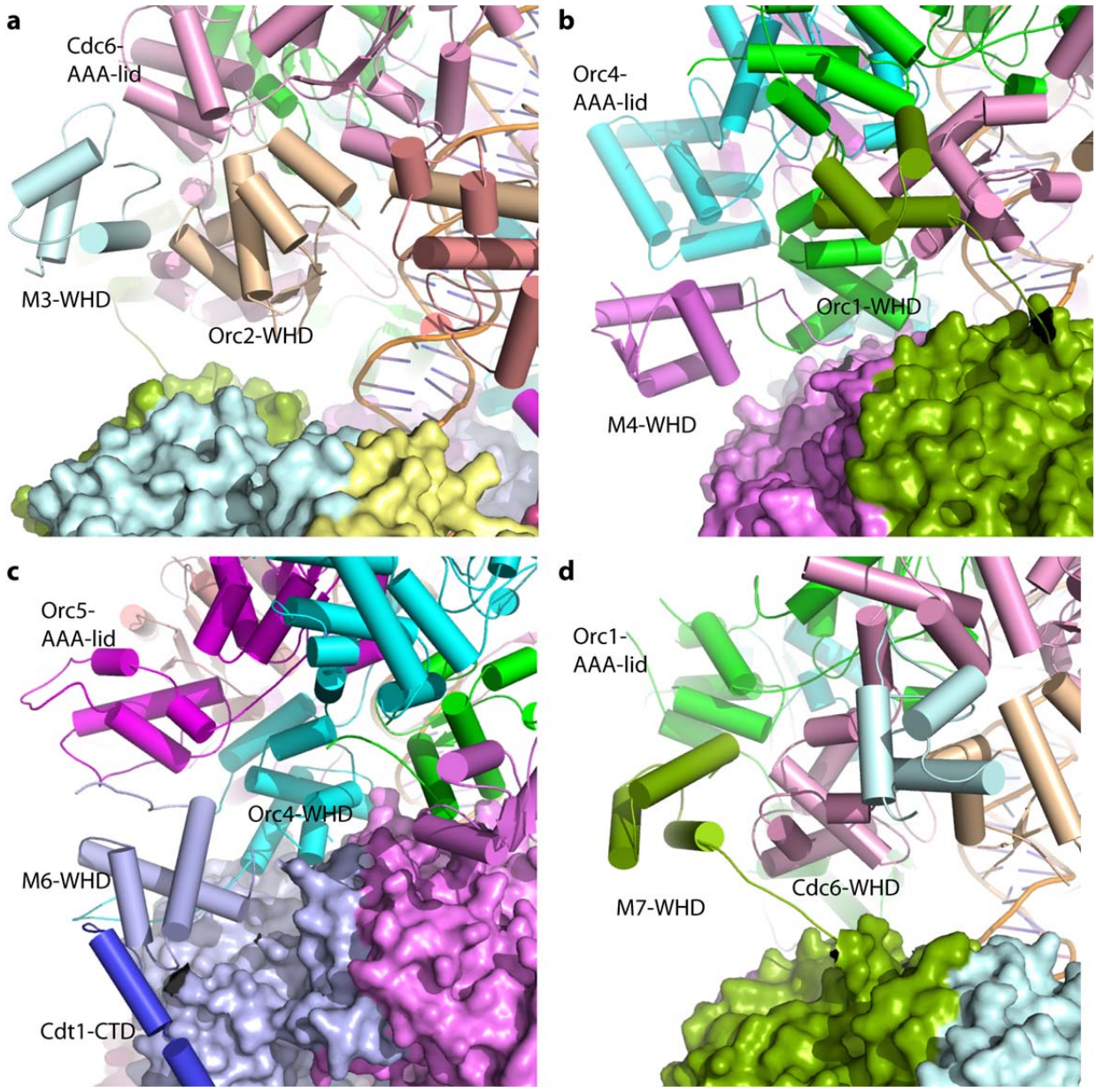
Supplementary Fig. 7. The dsDNA is loaded to the central channel of the Mcm2-7 hexamer. (**a**) Experimental density map of dsDNA is colored in brown. (**b**) Resolution map of the dsDNA density isolated from OCCM complex. (**c**) Atomic model of dsDNA is superimposed onto the DNA density map. The front density of OCCM is removed to shown the DNA density in the middle.



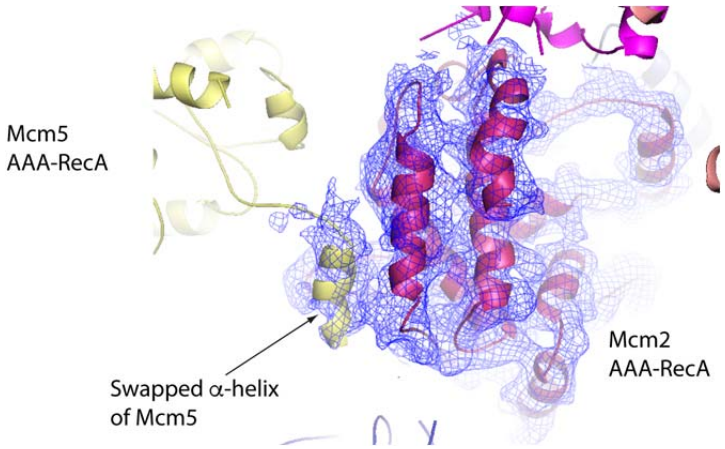
Supplementary Fig. 8. Nucleotide densities found at the interface between Mcm4-Mcm7, Mcm6-Mcm4, Mcm7-Mcm3, Mcm2-Mcm6, Orc1-Orc4, Orc4-Orc5, Orc5-Orc3, and Cdc6-Orc1. Protein structures are shown in cartoon, ATPγS in sticks, and electron densities of the nucleotides are shown in gray meshes.



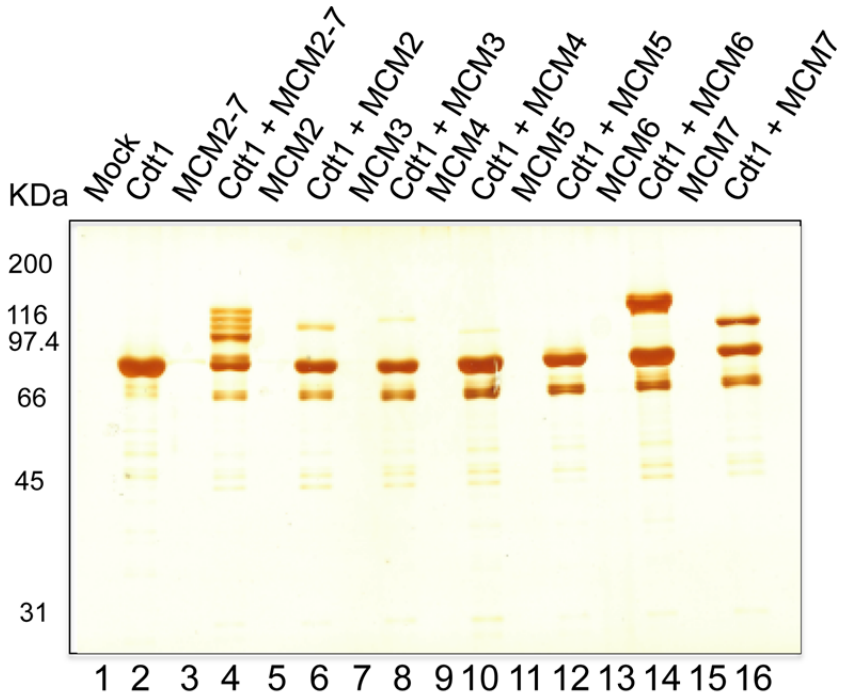
Supplementary Fig. 9. The position of the WHD of an Mcm protein varies greatly and sometimes can extend far away from the main body of the protein in OCCM. (**a**) Six Mcm protein structure. Mcm2 has no WHD, and Mcm5 WHD was flexible in OCCM. (**b**) The positions of the two resolved WHDs in CMG helicase. No WHD was modeled in the reported DH structure.



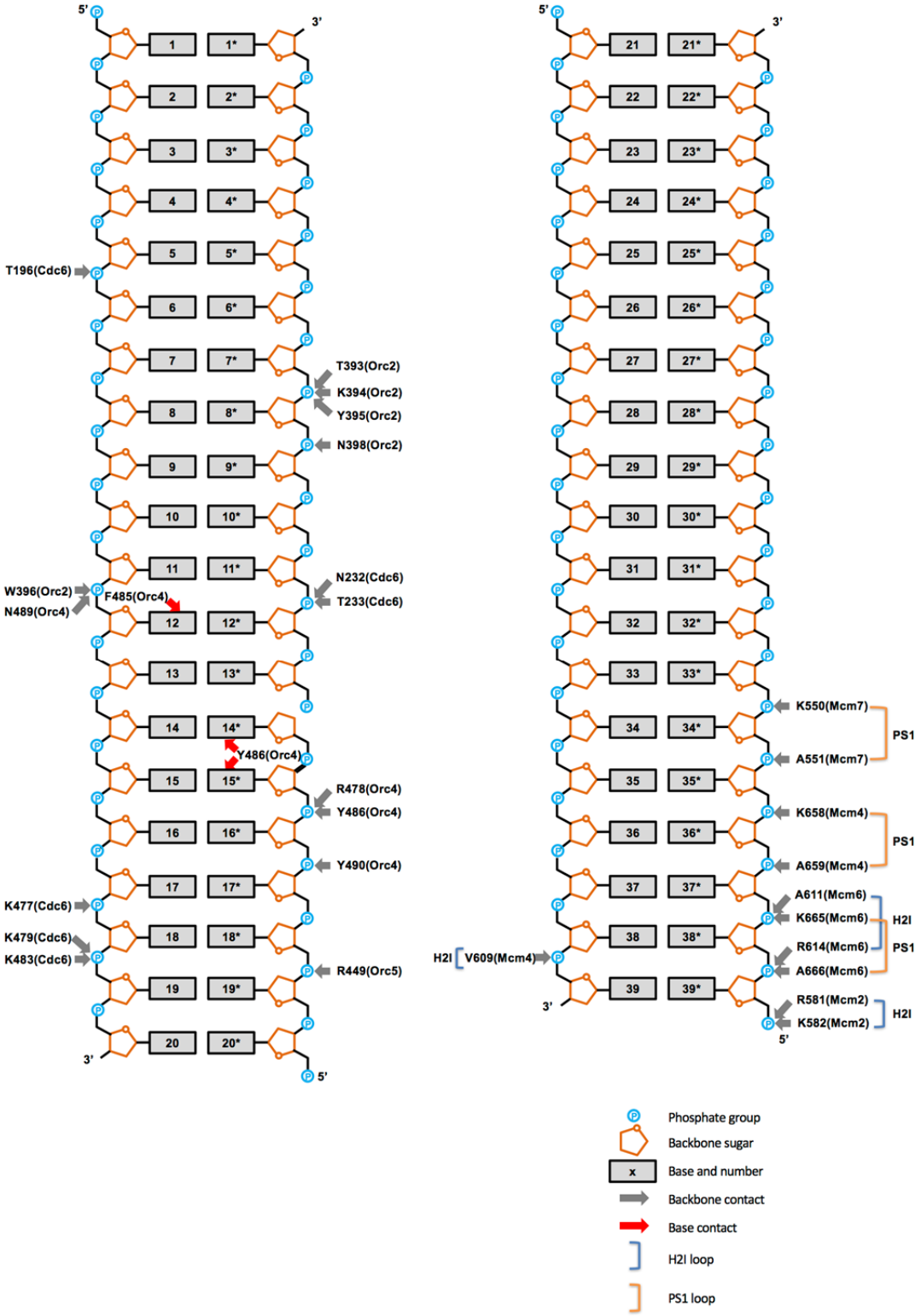
Supplementary Fig. 10. Interaction between ORC-Cdc6 loader ring and the four identified WHDs of Mcm3 (a), Mcm4 (b), Mcm6 (c) and Mcm7 (d). Each of the four Mcm WHDs binds to one WHD of a loader ring subunit and an AAA-lid domain of its neighbor subunit simultaneously, but their individual binding mode is distinct.



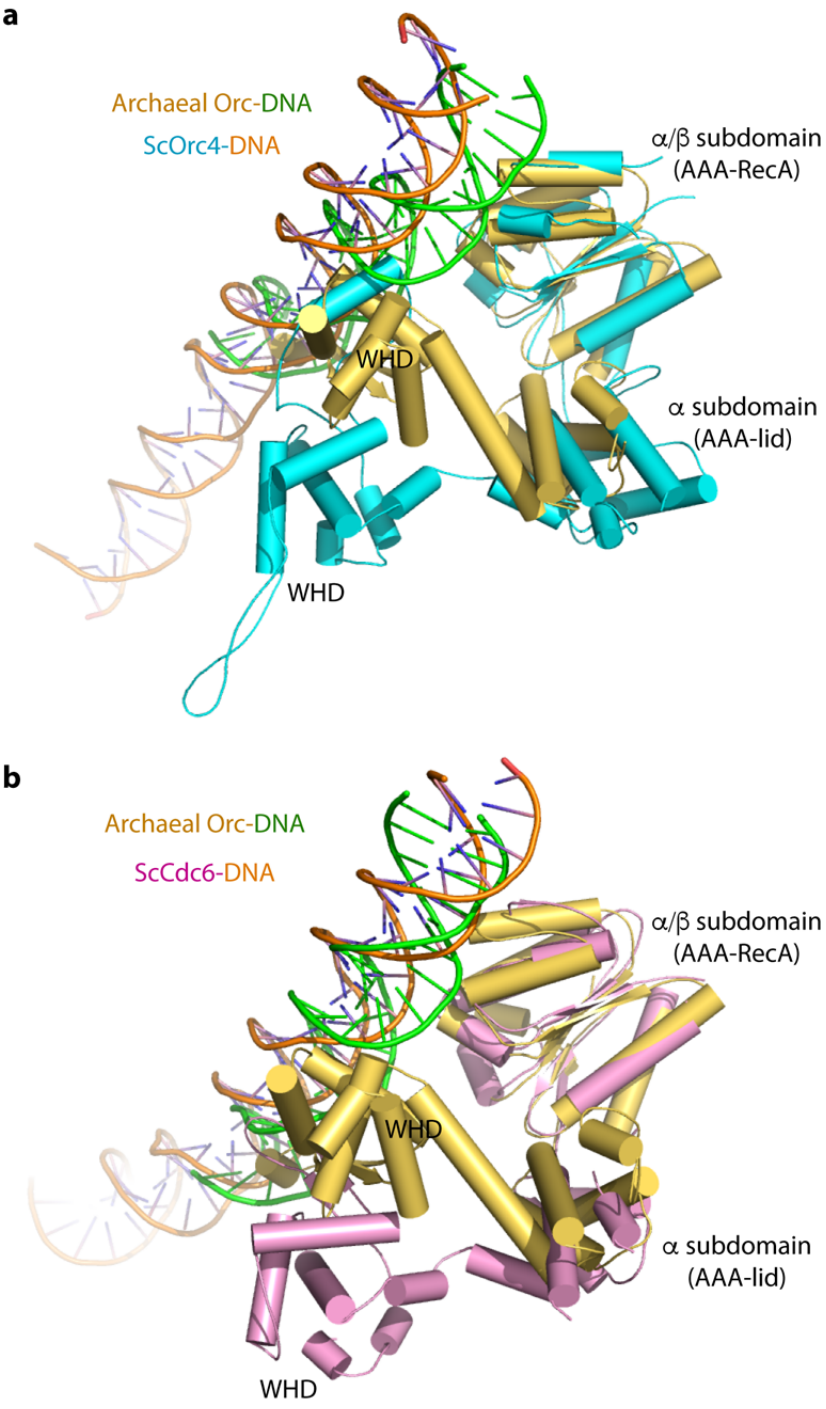
Supplementary Fig. 11. The Mcm2/5 gate is closed at the C-tier AAA+ region. Although the N-tier domains of Mcm2 and Mcm5 are separated by a gap, one α-helix in the Mcm5 AAA-RecA domain extends to and binds the AAA-RecA domain of Mcm2, indicating that the gate is closed at the C-tier region.



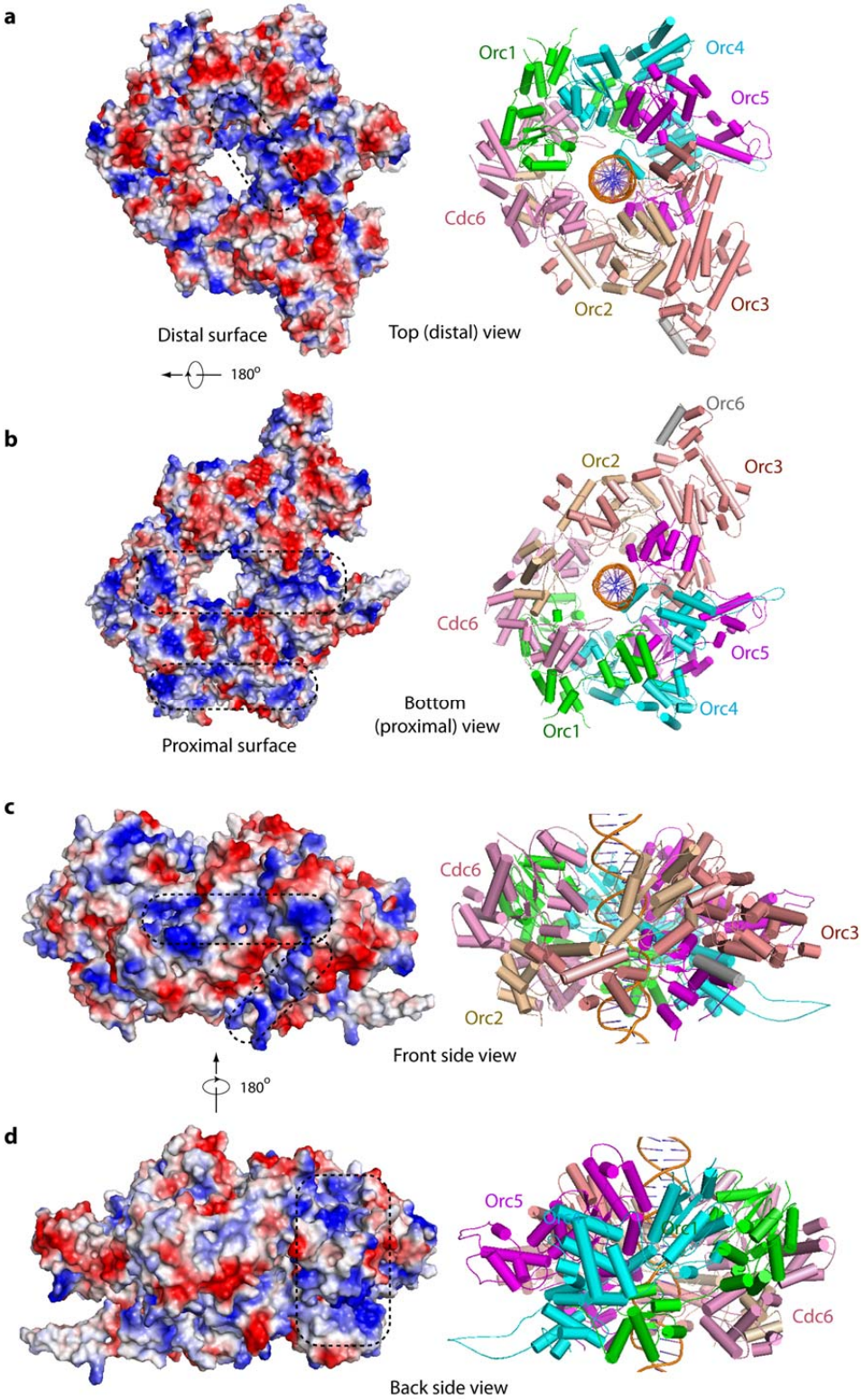
Supplementary Fig. 12. Analysis of Cdt1 Mcm2-7 subunit interaction. Cdt1 interacts with the Mcm2-7 complex as well as Mcm2, Mcm6 and Mcm7 subunits separately. Extracts from baculovirus infected Hi-Five cells containing Strep-Strep-SUMO tagged Cdt1 alone or with the Mcm2-7 complex or individual MCM subunits were precipitated with Strep-Tactin beads, washed, separated by gel electrophoresis and analyzed by silver-staining.



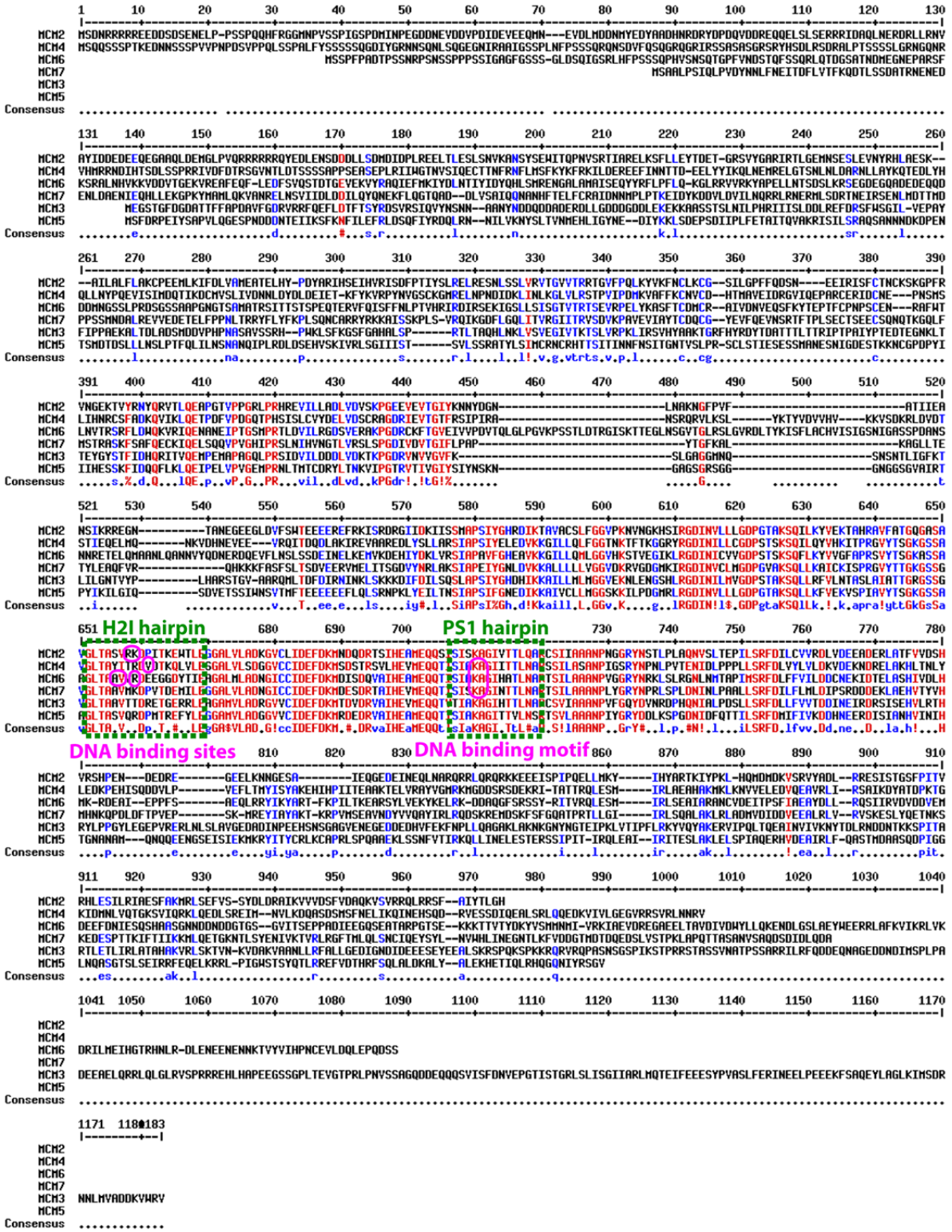
Supplementary Fig. 13. Detailed interaction between the protein subunits and the modeled 39-bp DNA. Left panel shows the first 20-bp DNA located in the top ORC-Cdc6 region. ORC-Cdc6 interact with both strands. Right panel shows the remaining 19-bp DNA. The PS1 and/or H2I loops of Mcm2,4,6, and 7 extensively interact with the last seven bases of the right strand.



Supplementary Fig. 14. Different DNA binding mode between yeast initiator protein Orc4 (a) and Cdc6 (b) and archaeal homologue Orc1/Cdc6 structure (PDB ID 2V1U). Unlike the WHD of the archaeal initiator which interacts with DNA, the WHDs of the yeast Orc4 and Cdc6 rotate 90° away from the Mcm hexamer DNA channel and do not interact with DNA.



Supplementary Fig. 15. Surface charge of the ORC-Cdc6 in top view that is distal to Cdt1-Mcm2-7 (a), in bottom view that is proximal to the C-tier ring of Mcm2-7 (b), in front side (c), and in back side view (d). The rounded rectangles mark several positive patches.



Supplementary Fig. 16. Multi-sequence alignment of Mcm2-7. Highlighted in dashed green squares and pink ovals are DNA binding elements. The DNA-binding KA motif in PS1 hairpin is highly conserved. The Mcm2, 4, 6, and 7 are group together to show the clustering of the DNA binding sites.